Supplementary Information for

Land use impacts the environmental benefits of wind energy farms in China

Kang Xu[1], Hanwen Zhu[2,3], Shuai Zhang[2,3], Mingming Wang[2,3], Wei Li[4], Wenji Zhou[5], Shuangcheng Li[6], Zhou Shi[2,3] & Jinfeng Chang[2,3]*

[1]Jiangsu Key Laboratory for Recognition and Remediation of Emerging Pollutants in Taihu Basin, School of Environmental Science and Engineering, Wuxi University, Wuxi, China

[2]Zhejiang Key Laboratory of Agricultural Remote Sensing and Information Technology, Zhejiang University, Hangzhou, China

[3]College of Environmental and Resource Sciences, Zhejiang University, Hangzhou, China

[4]Ministry of Education Key Laboratory for Earth System Modeling, Department of Earth System Science, Tsinghua University, Beijing, China

[5]Department of Energy Economics, School of Applied Economics, Renmin University of China, Beijing, China

[6]College of Urban and Environmental Sciences, Peking University, Beijing, China

* E-mail: changjf@zju.edu.cn

This file contains

Supplementary Methods

1.1. Detailed information of LCA framework

LCA has been widely used to evaluate environmental factors and potential impacts of a specific product system [1]. In accordance with the ISO 14040/44 standard, the LCA framework contains four main procedures: goal and scope definition, inventory analysis, impact assessment, and interpretation [2, 3]

Manufacturing is the only life cycle stage that is common to all LCA studies, including the raw material productions such steel, copper, and fiberglass. and the manufacturing of turbine components, foundations, and electrical connections. The installation stage usually includes indoor procedures (assemble the impellers, cabins, towers and flanges) and outdoor procedures (lay the foundations and site cables, erect the towers and turbines, and pave the roads). The operation and maintenance stage covers repair and replacement of parts, oil and lubricant changes, and transportation of these materials and technicians to wind farms [4]. Though some studies worked on the land-use area during installation [5, 6], few of them quantified the impacts of land-use by wind facilities such as carbon losses. Human-induced disturbances and impacts on soil and vegetation often causes a range of environmental issues, especially the GHG emissions and subsequent climate change [7-9]. The construction of impermeable surface will result in drastic soil carbon losses [10, 11] and vegetation carbon losses [12]. Furthermore, there may be a subsequent loss of additional carbon sink capacity during maintenance and operation stage due to the loss of soil and destruction of vegetation. Therefore, the GHG emissions and relative indices caused by land-use change should be integrated into the LCA frameworks. We considered the carbon storage loss caused by the changes of land type during the installation stage and the loss of additional carbon sink capacity caused by the destruction of the original ecosystem during the operation and maintenance stage. Specifically, in the installation stage, we estimated the carbon loss from the destruction of soil and vegetation caused by road construction and turbine foundation construction, the losses of soil organic carbon and vegetation carbon were integrated as land-use induced GHG emissions into the total emissions. In the maintenance and operation stage, we accounted for the total amount of loss of additional sink capacity (LASC) that can be achieved by soil and vegetation in the whole life cycle (20 years) without damage. We converted the LASC into land-use induced GHG emissions and integrated them into the total emissions.

1.2. Detailed information of the wind farms

In this study, we determined the impact area of the wind turbines by analyzing the changes in land use before and after installation. Upon reviewing the remote sensing images, it showed that certain areas, such as roads, open spaces, and cable zones, remained unaltered even after the installation. According to the distribution of China's wind energy (Supplementary Figure 2), we selected three wind farms located in forest, grassland, and desert, respectively. The remoting sensing images of the entire wind farms were illustrated in Supplementary Figure 3.

Forest ecosystem wind farm (FWF). We selected Shaobaishan wind farm, located in Yimei, Yichun, Heilongjiang Province, as a typical wind farm in the forest ecosystem (FWF). It belongs to a mid-temperate continental monsoon climate zone. The vegetation type is coniferous and broad-leaved mixed forest. Shaobaishan wind farm sited in the region with large carbon storage which play a crucial role in the national carbon budget of China [13]. It could be a typical example to study the impact of wind farms on ecosystems with carbon storage. The average altitude of the wind turbines installation is 900-1000 m. This wind farm is composed of 33 Gold Wind GW77-1500 KW wind turbines with a total installed capacity of 49.5 MW.

Grassland ecosystem wind farm (GWF). More than one-third wind turbines in China located in grassland (Supplementary Figure 2a), while Inner Mongolia has the largest wind capacity in the country [14]. We selected Dongshan wind farm, located in the west of Chifeng, Inner Mongolia, as a typical wind farm in the grassland ecosystem (GWF). It belongs to the plateau alpine region. The vegetation type is typical steppe with high plant diversity [15]. The average altitude of the wind turbines is 1650-1740 m. There are 100 large wind turbines (Vestas V80-2000 KW), with a total installed capacity of 200 MW.

Desert ecosystem wind farm (DWF). Guazhou, known as the "World Wind Library" [16], owns the largest wind farm cohort in the world, which provides an ideal case for studying the impacts of wind on desert ecosystems. We selected Guazhou Qiaowan wind farm, located in the northern part of Guazhou, Gansu Province, as a typical wind farm in the desert ecosystem (DWF). The land type belongs to Gobi Desert with sparse vegetation and low coverage. There are scattered annual grass and perennial shrubs such as *Bassia dasyphylla* (Fisch. et Mey.) O. Kuntze, *Nitraria sphaerocarpa* Maxim. and *Ephedra przewalskii* Stapf [17]. The altitude of wind turbines is 1300-1380 m. The DWF consists of 100 Dongfang FD77B-1500 KW wind turbines and 34 Gold Wind GW82-1500 KW wind turbines, with a total installed capacity of 201 MW.

1.3. Calculations

1.3.1. Power generation

Capacity factor: vertical wind speed changes due to the frictional effect at the surface of the earth. Based on the hourly wind speed data provided by the MERRA-2 meteorological data of the study area, we calculated the wind speed at the hub height v_h following the power law [18]:

$$v_h/v_0 = (h/h_0)^{\alpha} \quad (1)$$

which contains the wind speed as a function of the hub height h (unit: m), the scaling exponent α (unitless), the MERRA-2 wind speed v_0 (unit: m/s), and the displacement height of v_0 (2, 10 and 50 meters above ground). α equals to 1/7, and known as the wind shear exponent [19]. The estimated capacity factor cf is calculated from the wind speed $v_{h,t}$ at time t using the aggregate power curve PC_A for the given model of turbine:

$$cf_t = PC_A(v_{h,t}) \quad (2)$$

The average capacity factor was calculated as the product of the wind curtailment rate R_c and the average capacity factor of past 20 years (2001-2020):

$$cf = (1 - Rc)\,\frac{\sum_{t=1}^{n} cf_t}{n} \quad (3)$$

where n is the total number of hours from 2001 to 2020. The aggregate power curve was derived from turbine power curve PC_T which is provided the manufacturers. The PC_T was smoothed using a Gaussian filter Γ at the given point n (unit: m/s), and has mean zero and standard deviation related to wind speed by $\sigma = 0.6 + 0.2\, v$ [20]:

$$\Gamma(n,\sigma) = \frac{1}{\sqrt{2\Pi\sigma}} \exp\left(-\frac{n^2}{2\sigma}\right) \tag{4}$$

The aggregate power curve was evaluated at wind speed v (unit: m/s) from the integral of the turbine power curve multiplied by the filter Γ:

$$PC_A(v,\sigma) = \sum_{n=-4\sigma}^{4\sigma} PC_T(v-n)\ \Gamma(n,\sigma) \tag{5}$$

Supplementary Figure 4 shows the smoothed power curve of four wind turbines in three wind farms.

Total power generation: the total wind power generation (*PG*) among the entire life cycle was calculated as the product of the capacity factor, nominal power of turbine, turbine and lifetime

$$PG = P \times \sum_{i=1}^{8760\times 20} cf_i \tag{6}$$

where *P* represents the nominal power (unit: kW) of the wind turbine, 8760 represents the total number of hours per year, and 20 represents the service lifetime (unit: year). Accounting for the potential decline in wind turbine performance, the calculated *cf* values of wind farms were corrected based on the mean value from global studies on wind turbine performance decline (Supplementary Table 3) [21]. After careful evaluation, we excluded the 2014 UK study because its long-term dataset (spanning earlier turbine models) may overestimate degradation rates for modern turbines, which benefit from improved design and maintenance standards. For the remaining studies, we calculated the median decline rate, i.e. 0.53% per year, to correct the capacity factor in our analysis. We used the corrected *cf* values of 2001-2020 period as the capacity factors of the entire life cycle.

1.3.2. Land-use change induced carbon losses

Biomass carbon loss: we assumed that all the biomass carbon of direct occupation areas was lost due to the vegetation removal, which following:

$$CL_{biomass} = A \times CD_{biomass} \tag{7}$$

where $CL_{biomass}$ represents biomass carbon loss due to the construction of wind farms (unit: gC), A represents the direct land area occupied by wind power facilities (unit: m^2), and $CD_{biomass}$ represents the carbon biomass density (unit: gC m^{-2})

Soil organic carbon (SOC) loss: we used the CENTURY model [22], a widely used process-based soil carbon model, to quantify the SOC loss during the entire life cycle (20 years in this study). We assumed that there was no carbon input to SOC pool due to the impermeable surface of wind facilities, and SOC was mineralized constantly and returns to the atmosphere as CO_2. Driven by monthly average potential evapotranspiration, monthly average temperature and monthly average precipitation at the locations of the selected farms from China's monthly potential evapotranspiration dataset [23] and WorldClim dataset [24], The CENTURY model was first run to reach a steady-state where SOC input from vegetation and litter equal to the SOC loss from mineralization. The simulated SOC size was found comparable to that derived from Soil Database of China for Land Surface Modeling dataset (for the corresponding grid cell where the wind farms located) [25]. In a consecutive simulation, the carbon input to soil was set to 0 and the model was run for 20 years. Considering the ecological succession after construction, we simulated the offsetting of grassland plants in the second year of the overall life cycle. Subsequently, productivity recovered to 50% (with ANPP and BNPP recovering from 0% to 50% between the second and sixth years). The SOC losses during the 20 years of the life cycle of wind facility assumed in this study were calculated as:

$$CL_{soc} = A \times (SOCD_0 - SOCD_{20}) \tag{8}$$

where CL_{soc} represents the SOC loss without C input in 20 years (unit: g C), $SOCD_0$ and $SOCD_{20}$ represent the soil organic carbon density before and 20-years after wind power installation.

1.3.3. Greenhouse gas emissions

GHG emissions from carbon storage loss loss of carbon storage in the natural ecosystem, including the biomass carbon loss and SOC loss, was converted into greenhouse gas emissions (GHG_{CS}) due to land-use change. The formula is as follows:

$$\mathrm{GHG}_{CS} = \frac{44}{12}(CL_{biomass} + CL_{SOC}) \quad (9)$$

where $CL_{biomass}$ represents biomass carbon loss due to the construction of wind farms (unit: g C), CL_{soc} represents the SOC loss without C input in 20 years (unit: g C), and the coefficient 44/12 represents the relative molecular mass ratio of CO_2/C.

Life cycle GHG emissions from loss of additional sink capacity (LASC) due to the vegetation destruction caused by wind farm construction, the potential carbon sequestration by the original ecosystem is lost. The loss of additional sink capacity was converted into GHG emissions: GHG_{LASC}, and the formula is as follows:

$$\mathrm{GHG}_{LASC} = 20 \times A \times \frac{44}{12} \times \mathrm{NEP} \quad (10)$$

where NEP is the net ecosystem productivity of the original ecosystem (unit: g C m^{-2} y^{-1}), positive NEP indicate a net carbon sink of the ecosystem; 20 represents the service lifetime (unit: year) of the wind farm assumed in this study.

GHG emissions from materials and fuels the total consumption of raw materials and fuels used in the wind power system production is M_j (unit: gram), which was calculated as:

$$M_j = n \times \sum_{i=1}^{k} \sum_{j=1}^{t} M_{ij} \quad (11)$$

where n represents the number of turbine generators used in a wind farm, M_{ij} represents the consumption of the material j in stage i of a single wind turbine. According to the consumption of raw material M_j and the corresponding GHG emission factors, the industrial greenhouse gas emission GHG_M (unit: g CO_2-eq) was calculated as:

$$\mathrm{GHG}_{M} = \sum_{j=1}^{t} M_j \times C_j \quad (12)$$

C_j represents the GHG emission factor of unit raw material j.

Total GHG emissions and emission intensities the total greenhouse gas emissions (GHG_{total}) caused by the wind farm deployment was calculated as:

$$\mathrm{GHG}_{total} = \mathrm{GHG}_{M} + \mathrm{GHG}_{CS} + \mathrm{GHG}_{LASC} \quad (13)$$

The greenhouse gas emission intensity GHG_{int} (unit: g CO_2-eq·kWh^{-1}) is defined as the ratio between the total greenhouse gas emissions (GHG_{total}) and the total power generation *PG* (unit: kWh) during the entire life cycle of the wind farm, and is calculated as

$$\mathrm{GHG}_{int} = \frac{\mathrm{GHG}_{total}}{PG} = \frac{\mathrm{GHG}_{total}}{8760 \times 20 \times n \times cf \times P} \quad (14)$$

which contains the turbine number *n*, capacity factor *cf* and nominal power of the wind turbine *P*.

1.3.4. Land-use footprint

Land-use footprint accounts for the requirement of direct occupation area per unit of wind power generation. It is calculated as follows:

$$\mathrm{LUF} = \frac{A}{PG} \quad (15)$$

where *A* is the direct land area occupied by wind power facilities (unit: m^2), and *PG* is the wind power generation among the entire life cycle (unit: kWh).

Capacity density is a metric that describes the amount of direct occupation area that is needed to support per unit installed capacity (unit: MW). It is calculated as follows:

$$CD = \frac{P}{A} \quad (16)$$

where *P* represents the installed capacity (unit: MW) of the wind turbine, and *A* is the direct land area occupied by wind power facilities (unit: m^2).

1.3.5. Energy consumption and payback

Energy consumption the total energy consumption *E* (unit: MJ) was calculated as follows:

$$E = n \times \sum_{i=1}^{k} \sum_{j=1}^{t} M_{ij} \times e_i \times e_j \quad (17)$$

where e_j represents the energy input coefficient of unit raw material *j*, e_i represents the energy consumption coefficient for stage *i*, and *n* is the number of wind turbines.

Energy return on investment the energy return on investment *EROI* is defined as the total energy output divided by the total energy inputs. In this study, it was calculated using the total power generation *PG* and the total energy inputs *E* of the wind power farm's entire life cycle:

$$EROI = \frac{\text{Energy Output}}{\text{Energy Input}} = \frac{PG}{E} \tag{18}$$

Energy payback time energy payback time *EPT* (unit: year) is calculated as total energy consumption *E* divided by annual power generation as follows:

$$EPT = \frac{E}{PG/20} \tag{19}$$

1.4 Sensitivity analysis

We conducted sensitivity analysis in key factors and assumptions including the consumption of different materials (divided into three parts: steel & iron, cement and other materials), capacity factor, life time, land-use area and transport distance and curtailment rate. All land types related to three land type of China's wind farms to calculate the variation in wind capacity across different regions. Wind farms located in forests, grasslands, and deserts based on the locations of all wind farms in China [26]. Wind turbines and wind farms within a distance of 1km are considered as one wind farm, and we have identified a total of 128 forest wind farms, 141 grassland wind farms, and 124 desert wind farms (Supplementary Figure 5). Wind speed of all these wind farms was treated as input parameter to simulate the uncertainty of capacity factor. We estimated the power generation across land-use types for all 493 wind farms (standardized to 1.5MW turbine). This result reveals insignificant differences in generation capacity between forest, grassland, and desert sites ($p > 0.05$, Supplementary Figure 1). Monte Carlo was used to simulate the values of material consumption, life time, land-use area, transport distance and curtailment rate. The mean value and standardize value were based on previous research and dataset. For life time, mean and standard value was set to 20 and 3.5 [27]. For curtailment rate, mean and standard value was set to 0.0129~0.0769 and 0.0342 according to Chinese provincial curtailment rate provided by National Energy Administration. For distance, mean and standard value was set according to the provincial mean average distance from wind power industry bases to wind farms [28]. For land-use area, mean and standard value was set according to the research on land-use requirements of wind power in China [29]. For material consumption, mean value was set to the actual value of the selected wind farm and standard was set to 0.2*mean value.

1.5. Scenario design

Lifetime prolonging scenario ($S_{lifetime}$) Wind turbines are conventionally designed for a lifetime of 20 to 25 years. In this scenario, the lifetime was assumed to reach 25.4 years following the maximum lifetime expectancy (95% CI) of Denmark's wind turbines under scrapping schemes [30]. The annual inputs and outputs of extended service in operation longer than the design lifetime were assumed to be the same as that within the designed lifetime span.

Advanced manufacturing scenario ($S_{advanced}$) In this scenario, the main materials of wind facilities were assumed to be produced using advanced manufacturing technologies, while the emission factors and energy consumption factors were further reduced. Specifically, 1) a larger share of steel production using electric arc furnaces (~70%) with the GHG emission factor dropped to the Mexican level [31]; 2) iron was produced using direct reduced iron technology (following default assumptions in the 2006 IPCC guidelines); 3) copper was produced using secondary production copper [32]; 4) aluminum was produced using secondary production aluminum with the GHG emission factor dropped to the European level [33]; 5) silica was produced using continuous bioinspired processes [34]; 6) cement was produced from cement-based waste materials (clinker-to-cement ratio: 57%) [35, 36].

Clean manufacturing scenario (S_{clean}) In this scenario, the electricity consumption in the manufacturing stage was assumed to be produced from wind power instead of coal-fired power (with a GHG emission factor of 800 g CO_2-eq·kWh^{-1} in the baseline scenario; [31]). The emission factor of wind energy was used here following the national average in 2019 (19.88 g CO_2-eq·kWh^{-1}) [14]. As a result, over 16% of the GHG emissions of manufacturing stage could be further reduced.

Recycling and reuse scenario ($S_{recycling}$) In contrast to the assumption of all vegetation losses as CO_2 emissions in the baseline scenario, the felled trees due to the construction of wind facilities in the forest ecosystem (the FWF) in this scenario was assumed to be further recycled for wood products. Foliage and fruit mass of trees were not reused (the same as that in baseline solution), while stem mass was recycled and used for further wood products. The biomass allocation data to distinguish foliage, fruit, root and stem mass was from the dataset of global forests [37], and the water content and carbon content followed previous measurements [38] and IPCC default. For stem mass, we assumed that 87% of the stem mass was used for producing solid wood products (hardwood lumber) and 13% of that was used for manufacturing papers [39]. The displacement factor (tWHP/reducing tC) from meta-analysis [40, 41] and energy consumptions of manufacturing hardwood products based on LCAs [42] were used to quantify the GHG mitigation contributions and energy inputs for manufacturing solid wood products. The GHG emission factor and energy consumption factor of China's paper products were used to estimate the emissions and energy inputs of wood recycling [43, 44].

Land recovery scenario (S_{land}) In this scenario, two-thirds of the land occupation areas were assumed to be recovered by soil with 30 cm depth. It is assumed that the soil covering work took 1 hour on the area of 0.005 ha using VOLVO EC60B 37.4kW [45]. For the forest ecosystem, the recovering area was further implemented a reforestation project, and the extra energy inputs and LASC was quantified in this scenario [46].

Reduced curtailment scenario ($S_{curtailment}$) It is assumed that the curtailment rate of wind generations would reduce to 0.5% with no transmission constraints due to increasing transmission capacity and the rapid development of pumped hydro storage and electric boilers [47].

Large-scale (6MW) turbine deployment scenario (S_{6MW}) In this scenario, the existing wind turbines at the three sites were assumed to be upgraded with large-scale wind turbines Vestas V150 - 6 MW onshore turbines. The material breakdown of the turbine was obtained from the comprehensive life cycle inventory provided by Vestas, which facilitated a thorough life cycle assessment report [48]. The impact of land-use changes caused by larger turbine spacing distances as larger wind turbines was estimated based on the rotor diameter as follows:

$$\text{turbine spacing distance} = 0.39 * \text{rotor diameter}^{1.38} \quad (20)$$ [70]

Supplementary Table 1. Detailed information of wind farms and wind turbines.

Wind farm	Wind turbine	Rated power (MW)	Construction year	Rotor Diameter (m)	Hub height (m)	Cut-in wind speed (m/s)	Cut-out wind speed (m/s)
FWF	GW77-1500	1.5	2009	76.9	65	3.0	22.0
GWF	V80-2000	2	2010	80.0	78	4.0	25.0
DWF	GW82-1500	1.5	2009	82.3	70	3.0	22.0
	FD77B-1500	1.5	2008	77.0	65	3.0	20.0

Supplementary Table 2. Life cycle inventory of carbon emissions and energy consumptions.

Stage	Categories	GHG emission factors (kg CO_2/kg)	Energy consumption factors (MJ/kg)	Quantity			
				FWF	GWF	DWF	unit
Manufacturing	steel[31]	2.15	19.45	212631	371482	260892	kg/turbine
	iron[49]	1.95	17.66	37764	16898	0	kg/turbine
	copper[32]	5.88	81.72	36266	6159	25677	kg/turbine
	fiberglass[50, 51]	0.25	51.49	14246	7622	20298	kg/turbine
	aluminum[33]	21.60	49.80	0	2870	2738	kg/turbine
	silica[34, 51]	9.29	0.21	0	0	667	kg/turbine
	resin[49, 51]	2.72	32.33	21392	8594	2213	kg/turbine
	cement[35, 52]	0.47	4.90	1277070	1110743	936714	kg/turbine
Transportation	mass[51, 53, 54]			1599	1524	1249	t/turbine
	distance			2081	573	1697/1033	km
	trunk fuel[51]	2.96	46.03	62	16	36	t/turbine
	train fuel[51]	0.65	42.56	7	2	10	t/turbine

	garbage[55]	0.5 (kg/day person)		1217	1217	1217	kg/turbine
	distance			200	200	200	km
	harvest biomass[37, 38]	242 (tDM/ha)		117	0	0	t/turbine
	distance			400	400	400	km
Installation	area			0.38	0.37	0.62	ha/turbine
	vegetation removal[37, 56]	13.75 (kg/m3)	0.30	185	0	0	m3/turbine
	biomass C[57]			646	33	4	tC/ha
	SOC[25]			326	203	15	tC/ha
Operation and maintenance	carbon sink capacity[58, 59]			3.12	0.79	0.19	tC/ha yr
	copper replacement[60]	5.88	81.72	1269	216	899	kg/turbine
	silica replacement[60, 61]	9.29	0.21	0	0	100	kg/turbine
	steel replacement[60]	2.15	19.45	4831	8440	5927	kg/turbine
	fiberglass replacement[60]	0.25	51.49	4749	2541	6766	kg/turbine

	staff[62]	800 (g CO_2/kWh)	780 (kWh/yr person)	18.72	18.72	18.72	MJ/turbine
Disassembly and disposal	steel landfill[49, 56, 63, 64]	0.13	0.29	21263	37148	26089	kg/turbine
	iron landfill[49, 56, 63, 64]	0.13	0.29	3776	1690	0	kg/turbine
	copper landfill[49, 56, 63, 64]	0.13	0.29	1813	308	1284	kg/turbine
	fiberglass landfill[49, 56, 63-65]	0.13	0.29	14246	7622	20298	kg/turbine
	aluminum landfill[49, 56, 63, 64]	0.13	0.29	0	144	137	kg/turbine
	silica landfill[49, 56, 63, 64]	0.13	0.29	0	0	67	kg/turbine
	resin landfill[49, 56, 63, 64]	0.13	0.29	21392	8594	2213	kg/turbine
	steel recycling[49, 63, 64]			182	318	223	kg/turbine
	iron recycling[49, 63, 64]			32	14	0	kg/turbine
	copper recycling[49, 63, 64]			33	6	23	kg/turbine
	fiberglass recycling[63-66]			0	0	0	kg/turbine
	aluminum recycling[49, 63, 64]			0	3	2	kg/turbine
	silica recycling[49, 63, 64]			0	0	1	kg/turbine

Supplementary Table 3. Summary of global literature on wind turbine performance decline.

Reference	Year	Turbine type/location	Performance decline rate
How Does Wind Project Performance Change with Age in the United States	2020	U.S. turbines	0.53% per yr for the first 10 years, 1.27% per yr for the second 10 years, and a 3.6% year-10 drop
Analysis of Wind Turbine Aging through Operation Curves	2020	Vestas V52	8% in 10yr (ws 5-9 m/s) 1.3% in 10yr (ws 9-13 m/s)
A Study of Wind Turbine Performance Decline with Age through Operation Data Analysis	2020	Vestas V52	5% in 10yr
How does wind farm performance decline with age?	2014	UK's 282 wind farms	1.6 ± 0.2% per yr
Analysis of Wind Turbine Aging through Operation Data Calibrated by LiDAR Measurement	2021	IEC Class IIA 1 MW wind turbine	0.52% per yr
Wind turbine performance decline in Sweden	2017	Sweden wind turbines constructed before 2007	6% in 20yr

Have wind turbines in Germany generated electricity as would be expected from the prevailing wind conditions in 2000-2014?	2017	Germany wind turbines	0.63 ± 0.01% per yr
Data-driven wind turbine aging models	2021	Fifteen 2 MW wind turbines	0.2% per yr
Quantification of performance degradation due to wind turbine aging: Estimating the reduction in annual energy production using the annual degradation rate	2025	2.3 MW turbine	0.72% per yr
What drives the change of capacity factor of wind turbine in the United States?	2023	U.S. 943 wind farms	1.52% per yr

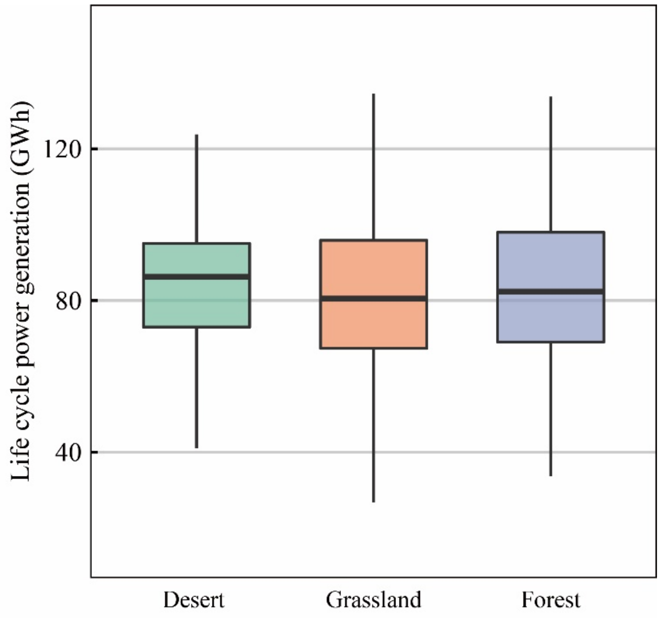

Supplementary Figure 1. Power generation across three land-use types for 493 wind farms in China.

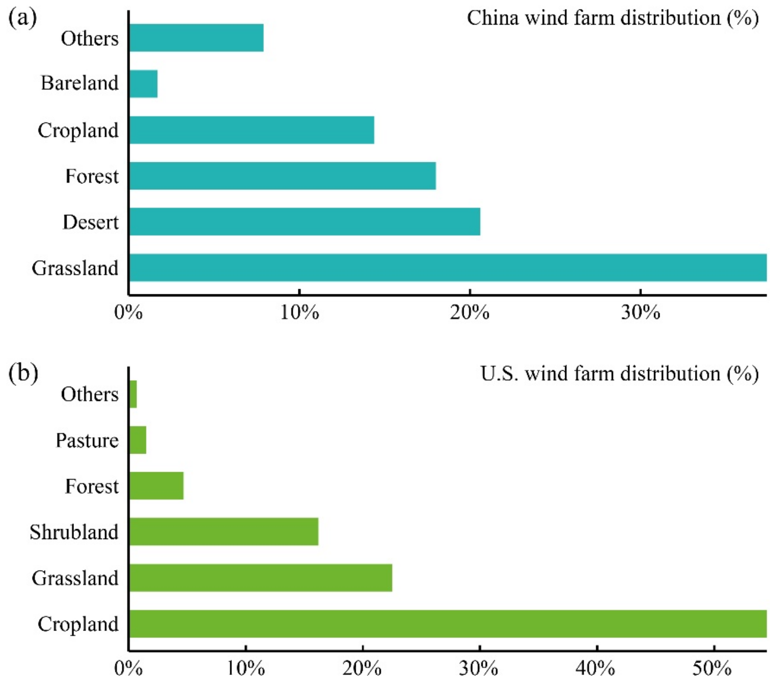

Supplementary Figure 2. Share of wind farms over different land cover types in (a) China and (b) the United States. Sources: harmonized global datasets of wind and solar farm [26]; Global land cover product (GLC_FCS30) [67]; U. S. Wind Turbine Database (UWSTDB) [68]; National Land Cover Database (NLCD) [69].

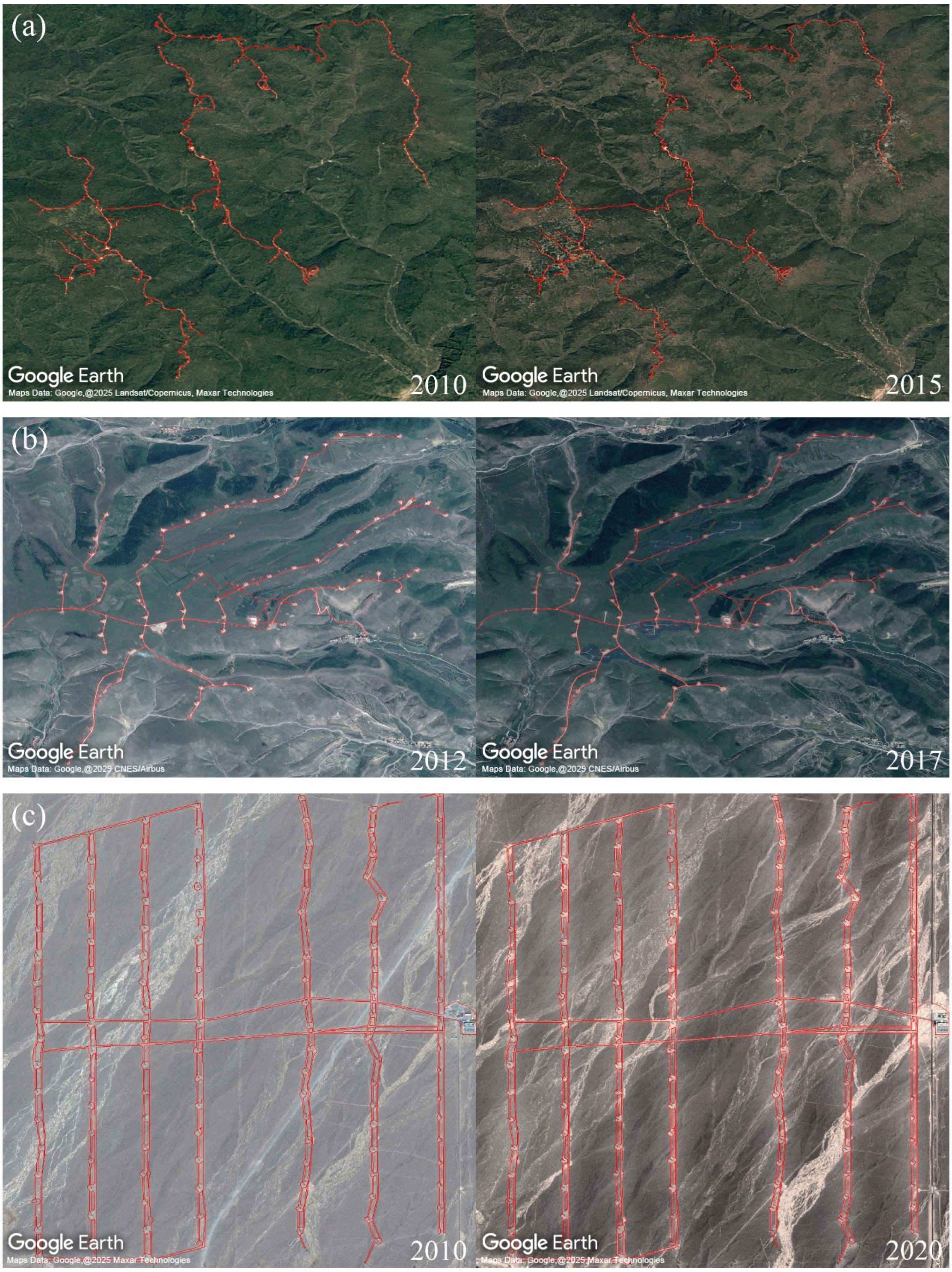

Supplementary Figure 3. The entire remote sensing images of (a) forest wind farm, (b) grassland wind farm, and (c) desert wind farm from Google Earth Pro (version 7.3.6.10201).

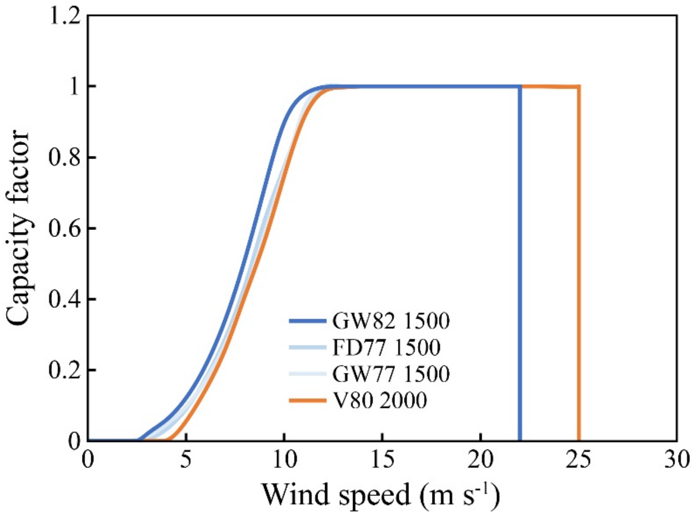

Supplementary Figure 4. Power curve models for GW82 1500, FD77 1500, GW77 1500 and V80 2000 onshore wind turbines.

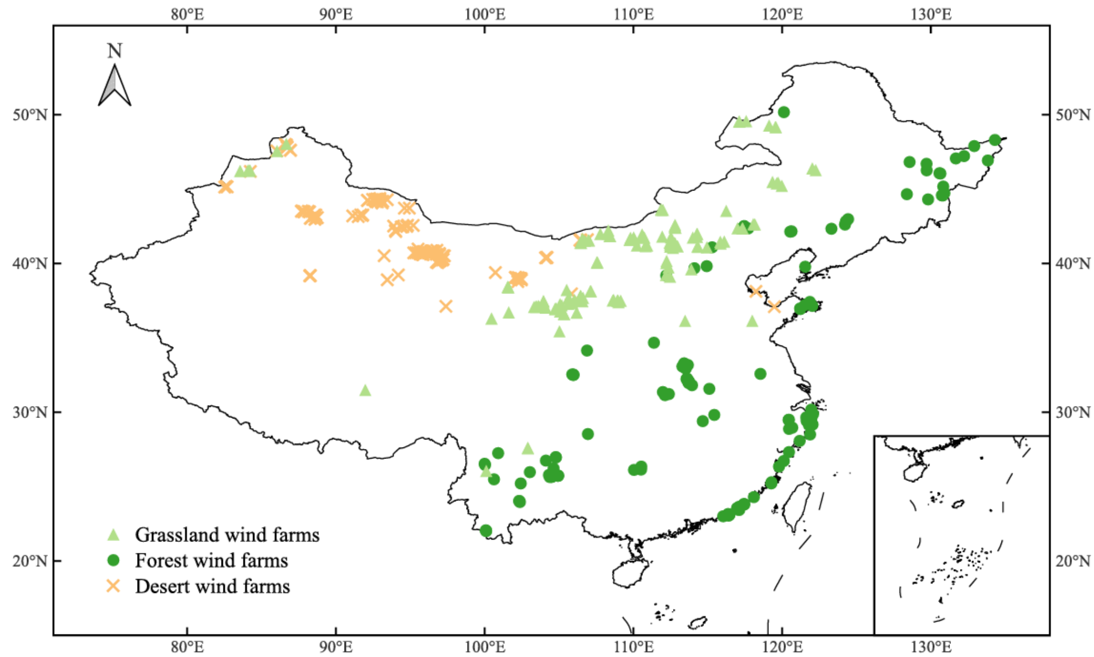

Supplementary Figure 5. The spatial distribution of China's 393 wind farms and their land cover types.

Supplementary References

1. Hellweg, S. & Canals, L.M.i. Emerging approaches, challenges and opportunities in life cycle assessment. *Science* **344**, 1109-1113 (2014).
2. ISO Environmental management – Life cycle assessment – Requirements and guidelines. Geneva, Switzerland: ISO. (2006).
3. ISO Environmental management – Life cycle assessment – Principles and framework. Geneva, Switzerland: ISO. (2006).
4. Teffera, B., Assefa, B., Björklund, A. & Assefa, G. Life cycle assessment of wind farms in Ethiopia. *The International Journal of Life Cycle Assessment* **26**, 76-96 (2020).
5. Rinne, E., Holttinen, H., Kiviluoma, J. & Rissanen, S. Effects of turbine technology and land use on wind power resource potential. *Nature Energy* **3**, 494-500 (2018).
6. Wachs, E. & Engel, B. Land use for United States power generation: A critical review of existing metrics with suggestions for going forward. *Renewable and Sustainable Energy Reviews* **143**, 110911 (2021).
7. Lai, L. et al. Carbon emissions from land-use change and management in China between 1990 and 2010. *Science Advances* **2**, e1601063 (2016).
8. Zeng, Y., Fang, N. & Shi, Z. Effects of human activities on soil organic carbon redistribution at an agricultural watershed scale on the Chinese Loess Plateau. *Agriculture, Ecosystems & Environment* **303**, 107112 (2020).
9. Feng, Y. et al. Modeling changes in China's 2000–2030 carbon stock caused by land use change. *Journal of Cleaner Production* **252**, 119659 (2020).
10. Chen, Y. et al. Changes in soil carbon pools and microbial biomass from urban land development and subsequent post-development soil rehabilitation. *Soil Biology and Biochemistry* **66**, 38-44 (2013).
11. Pekkan, O.I. et al. Assessing the effects of wind farms on soil organic carbon. *Environmental Science and Pollution Research* **28**, 18216-18233 (2021).
12. Tang, B. et al. The Observed Impacts of Wind Farms on Local Vegetation

Growth in Northern China. *Remote Sensing* **9**, 332 (2017).

13. Tang, X. et al. Carbon pools in China's terrestrial ecosystems: New estimates based on an intensive field survey. *Proceedings of the National Academy of Sciences* **115**, 4021-4026 (2018).
14. Xu, K. et al. A comprehensive estimate of life cycle greenhouse gas emissions from onshore wind energy in China. *Journal of Cleaner Production* **338**, 130683 (2022).
15. Sciences), C.C.A.o. Vegetation Atlas of China. (Science Press, Beijing, China; 2001).
16. Chang, R., Zhu, R. & Guo, P. A Case Study of Land-Surface-Temperature Impact from Large-Scale Deployment of Wind Farms in China from Guazhou. *Remote Sensing* **8**, 790 (2016).
17. Xu, K. et al. Positive ecological effects of wind farms on vegetation in China’s Gobi desert. *Scientific Reports* **9**, 6341 (2019).
18. Mentis, D., Hermann, S., Howells, M., Welsch, M. & Siyal, S.H. Assessing the technical wind energy potential in Africa a GIS-based approach. *Renewable Energy* **83**, 110-125 (2015).
19. Manwell, J.F., McGowan, J.G. & Rogers, A.L. Wind Energy Explained: Theory, Design and Application. (John Wiley & Sons, Ltd, Chichester, UK; 2009).
20. Staffell, I. & Pfenninger, S. Using bias-corrected reanalysis to simulate current and future wind power output. *Energy* **114**, 1224-1239 (2016).
21. Hamilton, S.D., Millstein, D., Bolinger, M., Wiser, R. & Jeong, S. How Does Wind Project Performance Change with Age in the United States? *Joule* **4**, 1004-1020 (2020).
22. Parton, W.J., Schimel, D.S., Cole, C.V. & Ojima, D.S. Analysis of Factors Controlling Soil Organic Matter Levels in Great Plains Grasslands. *Soil Science Society of America Journal* **51**, 1173-1179 (1987).
23. Peng, S. (ed. C. National Tibetan Plateau Data) (National Tibetan Plateau Data Center, 2022).

24. Fick, S.E. & Hijmans, R.J. WorldClim 2: new 1-km spatial resolution climate surfaces for global land areas. *International Journal of Climatology* **37**, 4302-4315 (2017).

25. Shangguan, W. et al. A China data set of soil properties for land surface modeling. *Journal of Advances in Modeling Earth Systems* **5**, 212-224 (2013).

26. Dunnett, S., Sorichetta, A., Taylor, G. & Eigenbrod, F. Harmonised global datasets of wind and solar farm locations and power. *Sci Data* **7**, 130 (2020).

27. Bech Abrahamsen, A. et al. Method for estimating the future annual mass of decommissioned wind turbine blade material in Denmark. *Wind Energy* **27**, 165-178 (2023).

28. Ruan, Z. et al. Spatiotemporal carbon footprint and associated costs of wind power toward China's carbon neutrality. *Resources, Conservation and Recycling* **205**, 107593 (2024).

29. Yang, N. et al. Land-use requirements and occupancy patterns of rapidly expanding wind power deployment in China. *Environmental Research Letters* **20** (2025).

30. MEGAVIND Strategy for Extending the Useful Lifetime of a Wind Turbine. (2016).

31. Hasanbeigi, A., Arens, M., Cardenas, J.C.R., Price, L. & Triolo, R. Comparison of carbon dioxide emissions intensity of steel production in China, Germany, Mexico, and the United States. *Resources, Conservation and Recycling* **113**, 127-139 (2016).

32. Dong, D., van Oers, L., Tukker, A. & van der Voet, E. Assessing the future environmental impacts of copper production in China: Implications of the energy transition. *Journal of Cleaner Production* **274** (2020).

33. Zhang, Y. et al. Environmental footprint of aluminum production in China. *Journal of Cleaner Production* **133**, 1242-1251 (2016).

34. Drummond, C., McCann, R. & Patwardhan, S.V. A feasibility study of the biologically inspired green manufacturing of precipitated silica. *Chemical*

Engineering Journal **244**, 483-492 (2014).

35. Wei, J. & Cen, K. Empirical assessing cement CO2 emissions based on China's economic and social development during 2001-2030. *Sci Total Environ* **653**, 200-211 (2019).
36. Sousa, V. & Bogas, J.A. Comparison of energy consumption and carbon emissions from clinker and recycled cement production. *Journal of Cleaner Production* **306**, 127277 (2021).
37. Michaletz, S.T., Cheng, D., Kerkhoff, A.J. & Enquist, B.J. Convergence of terrestrial plant production across global climate gradients. *Nature* **512**, 39-43 (2014).
38. Dias, D.P. & Marenco, R.A. Tree growth, wood and bark water content of 28 Amazonian tree species in response to variations in rainfall and wood density. *iForest - Biogeosciences and Forestry* **9**, 445-451 (2016).
39. Zhang, L., Sun, Y., Song, T. & Xu, J. Harvested Wood Products as a Carbon Sink in China, 1900-2016. *International Journal of Environmental Research and Public Health* **16**, 445 (2019).
40. Sathre, R. & O'Connor, J. Meta-analysis of greenhouse gas displacement factors of wood product substitution. *Environmental Science & Policy* **13**, 104-114 (2010).
41. Geng, A., Yang, H., Chen, J. & Hong, Y. Review of carbon storage function of harvested wood products and the potential of wood substitution in greenhouse gas mitigation. *Forest Policy and Economics* **85**, 192-200 (2017).
42. Bergman, R.D. & Bowe, S.A. Life-Cycle Inventory of Manufacturing Hardwood Lumber in Southeastern US. *Wood and Fiber Science* **44**, 71-84 (2012).
43. Chen, S., Yang, X., Li, Y., Cao, L. & Yue, W. Life-cycle GHG Emissions of Paper in China. *Journal of Beijing University of Technology* **40** (2014).
44. Zhao, G., You, Y. & Huang, Q. Carbon Footprint Assessment Method of Corrugated Medium on Life Cycle Assessment. *China Pulp & Paper* **40**, 40-44

(2021).

45. Qu, L. et al. Characteristics of PM2. 5 emissions and its carbonaceous components from construction machines under different typical driving modes. *Research of Environmental Sciences* **28**, 1047-1052 (2015).

46. Lefebvre, D. et al. Assessing the carbon capture potential of a reforestation project. *Sci Rep* **11**, 19907 (2021).

47. Jorgenson, J., Mai, T. & Brinkman, G. Reducing Wind Curtailment through Transmission Expansion in a Wind Vision Future. (2017).

48. Vestas (Vestas Wind Systems A/S, Hedeager 42, Aarhus N, 8200, Denmark; 2022).

49. Li, J., Li, S. & Wu, F. Research on carbon emission reduction benefit of wind power project based on life cycle assessment theory. *Renewable Energy* **155**, 456-468 (2020).

50. IPCC EFDB: 2006 IPCC default.

51. Gao, C. et al. Environmental impact analysis of power generation from biomass and wind farms in different locations. *Renewable and Sustainable Energy Reviews* **102**, 307-317 (2019).

52. Geng, Y., Wang, Z., Shen, L. & Zhao, J. Calculating of CO2 emission factors for Chinese cement production based on inorganic carbon and organic carbon. *Journal of Cleaner Production* **217**, 503-509 (2019).

53. Xu, L., Pang, M., Zhang, L., Poganietz, W.-R. & Marathe, S.D. Life cycle assessment of onshore wind power systems in China. *Resources, Conservation and Recycling* **132**, 361-368 (2018).

54. Li, L., Ma, X., Xie, M. & Liao, Y. Full Life Cycle Assessment on Wind Power Generation System. *Chinese Journal of Turbomachinery* **2**, 65-70+84 (2015).

55. Wind farm operation report (2021).

56. Steubing, B., Wernet, G., Reinhard, J., Bauer, C., & Moreno-Ruiz, E.. The ecoinvent database version 3 (part II): Analyzing LCA results and comparisonto version 2. *The International Journal of Life Cycle Assessment*, **21(9)**, 1269–

1281 (2016).

57. Spawn, S.A. & Gibbs, H.K. (ORNL Distributed Active Archive Center, 2020).

58. Zhang, L., Sun, R., Xu, Z., Qiao, C. & Jiang, G. Diurnal and seasonal variations in carbon dioxide exchange in ecosystems in the Zhangye oasis area, Northwest China. *PLoS One* **10**, e0120660 (2015).

59. Cai, H. et al. Carbon storage, net primary production, and net ecosystem production in four major temperate forest types in northeastern China. *Canadian Journal of Forest Research* **46**, 143-151 (2016).

60. Wang, X. Analysis on Environmental Benefit of Wind Turbines Using Life Cycle Assessment - Case Study of Some Wind Farm in Inner Mongolia. *Science and Technology Management Research* **18**, 259-262 (2012).

61. Li, H., Jiang, H.-D., Dong, K.-Y., Wei, Y.-M. & Liao, H. A comparative analysis of the life cycle environmental emissions from wind and coal power: Evidence from China. *Journal of Cleaner Production* **248** (2020).

62. Fan, Z., Lei, Y. & Wu, S. Research on the changing trend of the carbon footprint of residents' consumption in Beijing. *Environmental Science and Pollution Research* **26**, 4078-4090 (2019).

63. Chen, G.Q., Yang, Q. & Zhao, Y.H. Renewability of wind power in China: A case study of nonrenewable energy cost and greenhouse gas emission by a plant in Guangxi. *Renewable and Sustainable Energy Reviews* **15**, 2322-2329 (2011).

64. Yang, J. & Chen, B. Integrated evaluation of embodied energy, greenhouse gas emission and economic performance of a typical wind farm in China. *Renewable and Sustainable Energy Reviews* **27**, 559-568 (2013).

65. Heng, H., Meng, F. & McKechnie, J. Wind turbine blade wastes and the environmental impacts in Canada. *Waste Manag* **133**, 59-70 (2021).

66. Meng, F. et al. Comparing Life Cycle Energy and Global Warming Potential of Carbon Fiber Composite Recycling Technologies and Waste Management Options. *ACS Sustainable Chemistry & Engineering* **6**, 9854-9865 (2018).

67. Zhang, X. et al. GLC_FCS30: global land-cover product with fine classification

system at 30 m using time-series Landsat imagery. *Earth System Science Data* **13**, 2753-2776 (2021).

68. Hoen, B.D. et al. (ed. a.L.B.N.L.d.r. American Clean Power Association) (2018).

69. Yang, L. et al. A new generation of the United States National Land Cover Database: Requirements, research priorities, design, and implementation strategies. *ISPRS Journal of Photogrammetry and Remote Sensing* **146**, 108-123 (2018).

70. Dai, T. et al. Land Resources for Wind Energy Development Requires Regionalized Characterizations. *Environ. Sci. Technol.* **58**, 5014-5023 (2024).